IEEE Access
Multidisciplinary | Rapid Review | Open Access Journal

Received February 24, 2019, accepted April 16, 2019, date of publication May 1, 2019, date of current version May 23, 2019.

Digital Object Identifier 10.1109/ACCESS.2019.2912431

EKF Based Fuzzy PI Controlled Speed Sensorless Power Optimal Control of a Direct Drive Power System

JUNHUA YANG[1], BAOZHOU HUANG[1], HUI SHEN[2], DONGSHEN XIE[1], FENGJUN XIONG[1], SILING LU[1], AND HAIFENG CHEN[1]

[1]School of Automation, Guangdong University of Technology, Guangzhou 510006, China
[2]Maintenance Company of Henan Electric Power Corporation, Zhengzhou 450004, China

Corresponding author: Junhua Yang (YLY93@gdut.edu.cn)

This work was supported in part by the National Natural Science Foundation of China under Grant 51377026, in part by the Natural Science Foundation of Guangdong Province under Grant 2016B090912006, and in part by the Special Fund for Industry, University, and Research Cooperation of the Ministry of Education of Guangdong Province under Grant 2013B090500089.

ABSTRACT Faced with wave irregularity, the corrosion of the mechanical sensor in wave power generation systems, hazardous working conditions, and the inaccuracy of conventional control methods in the shifting system, a new type of irregular wave maximum wave energy capture strategy are proposed. The motivation behind the strategy is speed sensorless power optimal control of a direct drive wave power system by an extended Kalman filter (EKF) and self-tuning fuzzy proportional integral (PI) control. In our strategy, a fast Fourier transform (FFT) is utilized to analyze the spectrum of the irregular wave excitation force, and the maximum superposition control condition of the wave energy extraction is constructed by the vector superposition principle. Taking the voltage and current parameters of the generator as the input, based on two stages of prediction and update, an EKF observer system is established to estimate the speed and position of the power generation system. The fuzzy parameters are used to dynamically adjust the PI parameters so as to achieve optimal power state tracking control. The simulation results show that the FFT can meet the power optimal tracking requirements of unknown irregular waves. The proposed speed sensorless control scheme has good dynamic characteristics, small degree and position observation errors, and strong robustness, and allows the system to follow a given value.

INDEX TERMS Fast Fourier transform, wave power generation, linear permanent magnet synchronous generator, parameter self-tuning fuzzy PI, extended Kalman filter, optimal power.

I. INTRODUCTION

With the development of science and technology and the advancement of society, the demand for electricity is increasing, and the amount of nonrenewable energy is also increasing. The resulting environmental problems and lack of resources have gradually attracted the attention of the society.Therefore, new energy sources have gradually gained people's attention, and solar energy, wind power, and tidal energy have become an integral part of the world's power resources. As a green energy source with abundant content, a wide distribution and a high energy density [1], wave energy is highly developed in the world, with various applications in different fields, and the current research focuses on power generation and operation [2]. At present, wave power research mainly focuses on wave energy converter modeling [3], [4], wave energy extraction power optimization control [5], [6] and grid-connected operation control [7], [8].

Wave power generation systems with different structures are suitable for different sea conditions. Wave generators are available with both rotary and linear motors. According to the different forms of wave energy utilization, wave energy conversion devices can be divided into the pendulum type, over wave type, duck type, oscillating water column type, and fixed point suction type. This paper studies a direct-drive-type wave power generation device. The direct drive wave power generation system uses a linear permanent magnet

The associate editor coordinating the review of this manuscript and approving it for publication was Kuang Zhang.

synchronous generator (LPMSG) as the power generation carrier. The linear generator energy conversion device is integrated with the mover and generates electric energy by the relative displacement of the moving magnetic flux and the stator winding in the up and down direction of the wave. LPMSG requires only one level of energy conversion, is small in size, high in efficiency, and does not require frequent maintenance. It is more suitable for wave power generation than other rotating generators.The wave device is provided with a fixed mass and structure. When its natural frequency resonates with the wave frequency, the wave extraction power is theoretically the highest at this time. Reference [29] proposed a method to change the mass of the float to reach the resonance condition, but the mass change was a slow mechanical process, inconsistent with the timeliness of the motor control, and it was difficult to achieve maximum wave energy extraction. In [7], [8], the maximum power capture of irregular waves was analyzed. It was difficult to achieve maximum power capture by giving the excitation force of the known different frequencies and using the frequency of the dominant component for analysis control. In [9], the hydrodynamic equation of the wave device was equivalent to the circuit diagram. By using the principle of circuit resonance and controlling the anti-electromagnetic force parameters to achieve optimal power tracking, good results were obtained, but the control strategy was for a single known sine wave excitation force. For analysis, it did not apply to irregular waves.

Generator control requires detailed information on the position of the stator. However, the strong corrosiveness and complexity of the ocean presents a severe test for the maintenance of the mechanical speed sensors. Therefore, speed sensorless technology has unparalleled advantages in wave power applications. The currently widely used observation methods are: a sliding mode observer [10], [11], the model reference adaptive technique [12], high-frequency signal injection rotor position estimation [13], the Kalman filter observation method [14], and other new sensorless position control systems [15]. In order to overcome the limitations of the natural chattering of the sliding mode observer, [16] combined phase-locked loop technology and fuzzy control to improve the sliding mode, improve the observer robustness and reduce the chattering. Reference [17] used the adaptive gain algorithm to enhance the control precision of traditional sliding mode observers. Reference [18] used back electromotive (EM) force estimation, and [19] utilized the finite-state model of a predictive current control scheme to achieve position estimation. However, both were suitable for high-speed operation of the motor, the counter EM force generated in the long-term low-speed operation of the wave power system was very small, and the estimation error was large. References [20]–[22] proposed to use a Hall sensor with a low cost and small volume to detect the position of the rotor of the motor, but the limited number of sensors led to a low detection accuracy. At present, the EKF has been widely used in the speedless control strategies of permanent magnet synchronous linear motors [23], [24], achieving good tracking performance.

The classic proportional integral (PI) control technology is widely used in wave power system control due to its simplicity and reliability [8], [25]. However, a linear PI controller cannot achieve static tracking of sinusoidal signals, so it is difficult to meet the control requirements of a power generation system. Reference [26] used neural network (NN) adaptive dynamic surface control to reduce the tracking error. Reference [27] proposed a recursive wavelet fuzzy neural network and a robust adaptive backstepping sliding mode to control the speed, compensating for parameters and load disturbances. However, a neural network is the result of training iterations, so the iterative effect is sometimes good and sometimes poor. Reference [28] combined sliding mode variable structure control to realize motor control; tracking and adjustment of the speed were realized by the robustness and rapidity of the sliding mode variable structure, but the chattering of the sliding mode itself could not guarantee accurate tracking of the given signal.

In this paper, an FFT is used to obtain the optimal power capture conditions of an irregular wave excitation force through model mechanics analysis and the superposition principle. A simulation model of speed sensorless technology for a direct drive wave power generation system based on fuzzy PI control and an EKF observer is established. The LPMSG velocity is estimated by combining the stator voltage and current information, and the PI controller parameters are set in real time using a fuzzy algorithm. The simulation results show that the proposed optimal power strategy can satisfy the maximum efficiency of the wave energy conversion device for an irregular wave and obtain the maximum active power output. The speed sensorless control signal has a low signal velocity and a low position estimation error, robustness and a high following accuracy.

The body of this paper is organized as follows. In Section II, the principle of the maximum power capture strategy and the mathematical model of the LPMSG are analyzed to build a direct drive wave power system. The model's speed sensorless control technique is described in detail in Section III, which uses an EKF and a parametric self-tuning fuzzy PI controller. In order to verify the superiority of the method, the simulation results are explained and compared in Section IV. Finally, a conclusion is drawn in Section V.

II. DIRECT DRIVE WAVE POWER SYSTEM

A. REGULAR WAVE MAXIMUM POWER CAPTURE STRATEGY

A typical direct drive wave power system is shown in Fig. 1.

In view of the force of the float of the direct drive wave power system, the hydrodynamic equation of the wave energy capture device can be expressed as [7]:

$$m_t\ddot{x} + \beta_h\dot{x} + k_s x + F_e = F_w \tag{1}$$

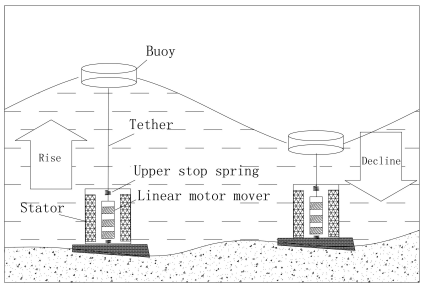

FIGURE 1. Schematic diagram of the direct drive wave power generation system.

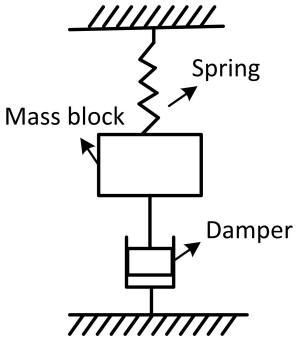

FIGURE 2. Mechanical model of the wave loading device.

where $\dot{x}$ is the velocity of the movement of the float and generator mover, x is the vertical displacement of the movement of the float, m_t is the total mass of the moving part, including the additional mass produced by seawater, β_h is the hydrodynamic damping coefficient of the converter, k_s is the elastic coefficient, F_w is the excitation force of the wave acting on the converter, and F_e is the electromagnetic force generated by the LPMSG.

The electromagnetic force can be written as:

$$F_e = R_g\dot{x} \tag{2}$$

where R_g is the damping coefficient of the active power generated by the motor.

Therefore, equation 1 can be written as:

$$m_t\ddot{x} + (\beta_h + R_g)\dot{x} + k_s x = F_w \tag{3}$$

The equation is analyzed for the excitation force of a single-frequency sinusoidal waveform. Assuming $F_w = F_0 sin(\omega t)$, equation 3 can be written as:

$$m\ddot{x} + c\dot{x} + kx = F_0 sin(\omega t) \tag{4}$$

where $m = m_t$, and $c = \beta_h + R_g$, $k = k_s$, ω is the wave angular velocity.

As shown in Fig. 2, the mathematical model can be equivalent to a linear combination of a linear spring, mass, and linear damper.

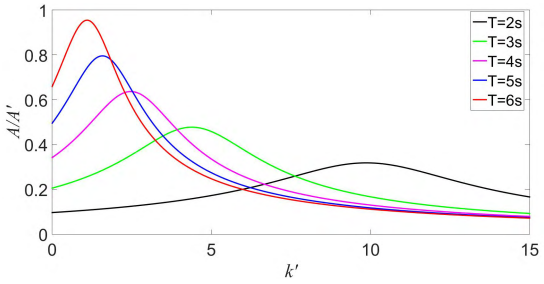

FIGURE 3. Motion displacement amplitude of the float.

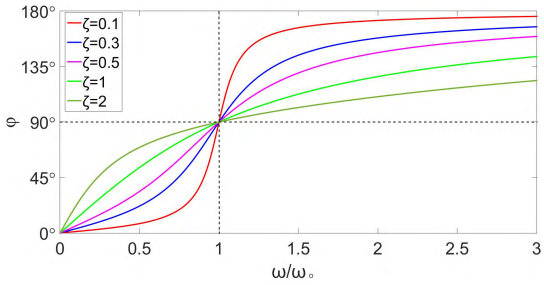

FIGURE 4. The phase of the motion displacement hysteresis of the float.

By solving equation 4, the motion displacement and phase of the mass can be obtained as:

$$\begin{cases} x = Asin(\omega t - \varphi) \\ A = \dfrac{F_0}{\sqrt{(k - m\omega^2)^2 + (c\omega)^2}} \\ \varphi = arctan\dfrac{c\omega}{k - m\omega^2} \end{cases} \tag{5}$$

Equation 5 can be converted into:

$$\begin{cases} A/A' = \dfrac{1}{\sqrt{k' - \mu^2)^2 + \mu^2}} \\ \varphi = arctan\dfrac{2\xi\omega/\omega_0}{1 - (\omega/\omega_0)^2} \end{cases} \tag{6}$$

where $A' = mF_0/c^2$, $k' = km/c^2$, $\mu = m\omega/c$, $\omega_0 = \sqrt{k/m}$, and $\xi = c/(2\sqrt{mk})$.

According to equation 6, the motion displacement amplitude and the lag phase diagram are shown in Fig. 3 and Fig. 4, as can be seen from Fig. 3, the excitation energies of different periods correspond to different maximum amplitudes. It can be clearly seen from Fig. 4 that the maximum amplitude position corresponds to the k value $k = m\omega^2$, which is $\omega/\omega_0 = 1$; at this time, the phase corresponding to the displacement phase lags behind the excitation force by 90^0. Therefore, when the switching device and the wave resonate, the speed remains in phase with the exciting force.

In a three-phase stationary coordinate system, the instantaneous power of the wave generation system is expressed as:

$$P = u_a i_a + u_b i_b + u_c i_c \tag{7}$$

where u_a, u_b, u_c; i_a, i_b, i_c are the voltage and current of the abc three phases of the generator, respectively.

If the internal loss of the generator is neglected, the instantaneous power can be replaced by $P = F_e\dot{x}$. When the mass achieves the resonance condition, $k = m\omega^2$. Then,

$$P=(R_g\dot{x})*\dot{x}=-n\omega^2 sin^2(\omega t)(A-\frac{m\omega F_0}{2kn})^2+\frac{(m\omega F_0)^2}{4k^2n} \quad (8)$$

In summary, the conditions for capturing the maximum power in the wave are: $k_s = m\omega^2$ and $R_g = n$.

B. IRREGULAR WAVE MAXIMUM POWER CAPTURE STRATEGY

In the actual ocean, the excitation force is superimposed by unequal-length sine and cosine signals, and there is external interference. The abovementioned proposed power optimal scheme is based on a known excitation frequency. Therefore, by combining digital signal processing ideas and considering data as discrete signals, we propose the use of a discrete FFT method to analyze the signal spectrum and extract the frequency component of the irregular excitation force.

The discrete Fourier transform of an N-point sequence x(n) is:

$$x(k)=\sum_{n=0}^{N-1}x(n)W_N^{kn} \quad (9)$$

where $k = 0, 1, \ldots, N-1$, and $W_N^{kn} = e^{-j2\pi/N}$.

The spectrum of a finite-length order excitation signal can be discretized into a finite-length sequence by the discrete Fourier transform (DFT), but the calculation of the DFT increases exponentially with an increase in the number of signal collection points, which makes it difficult to realize real-time processing. Finally, the FFT algorithm was introduced. The FFT takes advantage of the symmetry and periodicity of W_N and decomposes the long sequence of the DFT into several short sequences, which greatly reduces the amount of computation. Taking the base 2-FFT as an example, $X(k)$ is divided into two subsequences $X_1(k)$ and $X_2(k)$.

$$\begin{cases} X_1(k)=[X(0),X(2),\ldots,X(N-2)] \\ X_1(k)=[X(1),X(3),\ldots,X(N-1)] \end{cases} \quad (10)$$

where $k = 0, 1, \ldots, (N-1)/2$.

Equation 9 can be converted into:

$$\begin{aligned} x(k) &= \sum_{n=0}^{N/2-1}x_1(n)W_{N/2}^{kn}+W_N^k\sum_{n=0}^{N/2-1}x_2(n)W_{N/2}^{kn} \\ &= X_1(k)+W_N^kX_2(k) \end{aligned} \quad (11)$$

According to the idea of the FFT, an unknown frequency excitation force is decomposed into several frequency sinusoidal waveforms and a noise superposition, and the main frequency content of the wave is analyzed to obtain a sine wave at a series of frequencies:

$$F_w=F_w^1+F_w^2+F_w^3+\cdots+F_w^n \quad (12)$$

According to Equation 3, it can be decomposed into the following:

$$\begin{cases} m_t\ddot{x}_1+(\beta_h+R_g^1)\dot{x}_1+k_s^1x_1=F_w^1 \\ m_t\ddot{x}_2+(\beta_h+R_g^2)\dot{x}_2+k_s^2x_2=F_w^2 \\ \cdots\cdots \\ m_t\ddot{x}_n+(\beta_h+R_g^n)\dot{x}_n+k_s^nx_n=F_w^n \end{cases} \quad (13)$$

The control conditions for constructing the maximum power capture by the superposition principle are:

$$F_{emax}=R_g^1\dot{x}_1+R_g^2\dot{x}_2+R_g^3\dot{x}_3+\cdots+R_g^n\dot{x}_n \quad (14)$$

Since the electromagnetic force is directly related, the current can be controlled to meet the requirement of generating the maximum active power.

C. MATHEMATICAL MODEL OF THE LPMSG

Regardless of the magnetic circuit saturation problem of the generator, ignoring the end effect of the linear motor, and not counting losses such as hysteresis and the eddy current, the mathematical model of the d-q axis of the LPMSG can be obtained as follows:

$$\begin{cases} u_d=R_si_d+L_d\dfrac{\mathrm{di_d}}{\mathrm{d}t}-\dfrac{\pi}{\tau}vL_qi_q \\ u_q=R_si_q+L_q\dfrac{\mathrm{di_q}}{\mathrm{d}t}+\dfrac{\pi}{\tau}vL_di_d+\dfrac{\pi}{\tau}v\Psi_f \end{cases} \quad (15)$$

where u_d, u_q, i_d, i_q, L_d and L_q are the stator voltages, currents and inductances in the d-q coordinate system, respectively, R_s is the stator resistance, v is the speed, τ is the pole distance, and Ψ_f is the permanent magnet flux linkage.

The electromagnetic force equation of the generator is:

$$F_e=\frac{3\pi}{2\tau}n_p(\Psi_fi_q-(L_q-L_d)i_di_q) \quad (16)$$

where n_p is the pole logarithm.

The direct-drive-type wave power system generator mover and the wave converter float are integrated, so the converter mathematical equation 3 is also the mechanical motion equation of the generator.

For the sake of simple control, the mathematical model of the generator is decoupled by the method of feed-forward voltage compensation. The mathematical model of the LPMSG after decoupling is:

$$\begin{cases} u_{d0}=u_d+\dfrac{\pi}{\tau}vL_qi_q=R_si_d+L_d\dfrac{\mathrm{di_d}}{\mathrm{d}t} \\ u_{q0}=u_q-\dfrac{\pi}{\tau}vL_di_d-\dfrac{\pi}{\tau}v\Psi_f=R_si_q+L_q\dfrac{\mathrm{di_q}}{\mathrm{d}t} \end{cases} \quad (17)$$

III. SPEED SENSORLESS CONTROL TECHNOLOGY

A. EXTENDED KALMAN FILTER OBSERVER

The traditional estimation algorithm is generally suitable for high-speed operation systems. It has low detection accuracy of rotor position and speed at zero speed and low speed operation, and most of them are offline calculations, and are not real-time. The EKF optimal estimation filtering algorithm has a wide operating speed range. The speed estimation can

be completed in the high-performance servo system and the low-speed direct-drive wave power generation system, and the algorithm calculation can be performed in the data acquisition process, and the system state can be estimated online to realize real-time control.The algorithm has good dynamic performance, fast convergence speed and high prediction accuracy, while other improved EKF implementations are more complicated.

If a rotating coordinate system is used, the speed sensorless algorithm and the stator voltage and current measurements need to be converted to synchronous rotating coordinates; the transformation matrix will contain sine and cosine functions, which increase the nonlinearity of the mathematical model and increases the calculation time. A static coordinate system can avoid these problems. Therefore, this paper uses a mathematical model of the generator in a stationary coordinate system. The following equations of state can be obtained from equations 3 and 17:

$$\begin{cases} \dfrac{\mathrm{d}x}{\mathrm{d}t} = f(x) + Bu \\ y = Cx \end{cases} \tag{18}$$

$$f(x) = \begin{bmatrix} -\dfrac{R}{L_s} i_\alpha + d\dfrac{\pi\Psi_f}{\tau L_s} sin\theta_e \\ -\dfrac{R}{L_s} i_\beta - d\dfrac{\pi\Psi_f}{\tau L_s} cos\theta_e \\ \dfrac{\tau}{m_t\pi}[-d\dfrac{3\pi}{2\tau}\Psi_f(i_\beta cos\theta_e - i_\alpha sin\theta_e) - n\dot{x} - \dfrac{k_s\tau}{\pi}\theta_e] \\ \dfrac{\tau}{\pi}\dot{x} \end{bmatrix} \tag{19}$$

where $x = \begin{bmatrix} i_\alpha & i_\beta & \dot{x} & \theta_e \end{bmatrix}^T$, $u = \begin{bmatrix} u_\alpha & u_\beta & \dfrac{\pi n_p F_w}{m_t \tau} \end{bmatrix}^T$, $y = \begin{bmatrix} i_\alpha & i_\beta \end{bmatrix}^T$, $B = \begin{bmatrix} 1/L_s & 0 & 0 \\ 0 & 1/L_s & 0 \\ 0 & 0 & 1 \\ 0 & 0 & 0 \end{bmatrix}$, and $C = \begin{bmatrix} 1 & 0 & 0 & 0 \\ 0 & 1 & 0 & 0 \end{bmatrix}$.

The state estimation of the EKF consists of two phases: prediction and update. In the first stage, the state of the next moment is estimated mainly by the state estimation of the current moment. The second phase is mainly to update the estimated value based on the current observations. The specific steps are:

(1) Predict the state of the vector;

Predict the state vector value at time (k+1) by inputting u(k) and the value of the last state estimate. The equation is:

$$\tilde{x}(k+1) = \hat{x}(k) + T_s[f(\hat{x}(k)) + Bu(k)] \tag{20}$$

where T_s is the sampling period, $'\hat{}'$ indicates the state estimation, and $'\tilde{}'$ indicates the predicted value.

(2) Calculate the output corresponding to the predicted amount at this time;

$$\tilde{y}(k+1) = C\tilde{x}(k+1) \tag{21}$$

(3) Calculate the error covariance matrix;

$$\tilde{P}(k+1) = \hat{P}(k) + T_s[F(k)\hat{P}(k) + \hat{P}(k)F^T(k)] + Q \tag{22}$$

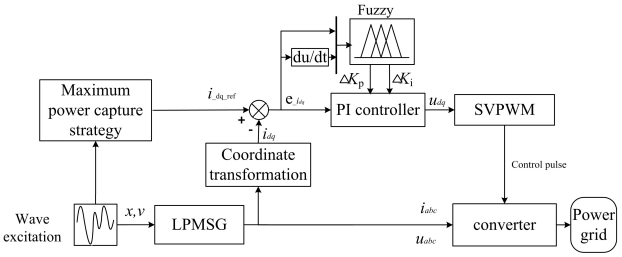

FIGURE 5. Schematic diagram of self-tuning fuzzy PI control.

where:

$$F(x) = \frac{\partial f(x)}{\partial x}|_{x=\hat{x}(k)}$$

$$= \begin{bmatrix} -\dfrac{R}{L_s} & 0 & \dfrac{\Psi_f}{L_s} sin\hat{\theta}_e(k) & \dfrac{\pi\Psi_f}{\tau L_s}\hat{\dot{x}}(k) cos\hat{\theta}_e(k) \\ 0 & -\dfrac{R}{L_s} & -\dfrac{\Psi_f}{L_s} cos\hat{\theta}_e(k) & \dfrac{\pi\Psi_f}{\tau L_s}\hat{\dot{x}}(k) sin\hat{\theta}_e(k) \\ \eta sin\hat{\theta}_e(k) & -\eta cos\hat{\theta}_e(k) & -\dfrac{n}{m_t} & \hat{\gamma}(k) \\ 0 & 0 & 1 & 0 \end{bmatrix} \tag{23}$$

$$\hat{\gamma}(k) = \eta\hat{i}_\alpha(k) cos\hat{\theta}_e(k) + \eta\hat{i}_\beta(k) sin\hat{\theta}_e(k) - \frac{k_s}{m_t} \tag{24}$$

$$\eta = \frac{3\pi^2 n_p^2}{2m_t\tau^2}\Psi_f \tag{25}$$

(4) Calculate the gain matrix;

$$K(k+1) = \tilde{P}(k+1)C^T[C\tilde{P}(k+1)C^T + R]^{-1} \tag{26}$$

(5) Update the state variables;

$$\hat{x}(k+1) = \tilde{x}(k+1) + K(k+1)[y(k+1) - \tilde{y}(k+1)] \tag{27}$$

This step is the corrected state estimation, which is filtering.

(6) Update the covariance matrix;

$$\hat{P}(k+1) = \tilde{P}(k+1) = K(k+1)C\tilde{P}(k+1) \tag{28}$$

B. SELF-TUNING FUZZY PI CONTROLLER DESIGN

1) DESIGN CONTROLLER

It can be seen from Equation (14) that the ultimate control objective of the maximum power capture control strategy of the direct drive wave power generation system is to make the Q-axis current meet the given value under the current conditions, with a fast response speed and strong anti-interference ability. Accordingly, the electromagnetic force of the generator satisfies the resonance requirement of the wave device, because the waves are randomly changing, given a current time-varying target. It is difficult for a fixed PI controller to achieve no dead tracking. By using fuzzy reasoning to realize dynamic online self-tuning of the PI parameters, the controller can be automatically corrected in a random environment, with good dynamic and static performance, a small calculation and easy real-time control.

The self-tuning fuzzy PI control principle is shown in Fig. 5. The main goal of the current loop is to make the actual output current of the generator quickly follow the current expected value obtained by the FFT-based maximum power capture control strategy analysis. That is to say, the main performance indicator is the current tracking error. Therefore, the fuzzy controller takes the current error e and the error rate of change de/dt as inputs, uses the dynamic adjustment of the PI parameter ΔK_p and ΔK_i as the output variable, and combines the PI controller to form the parameter self-tuning fuzzy PI controller, which outputs the power generation. The machine expects current. The SVPWM control strategy is used to control the switch-on of the machine-side converter, thereby outputting the maximum active power of the direct drive wave power system.

2) FUZZY RULE SELECTION

In general, the number of elements in the domain is more than twice the total number of fuzzy subsets, to ensure the coverage of the fuzzy subsets and to avoid runaway. Taking into account the accuracy of the algorithm and the amount of calculation, the three levels of "large, medium and small" are used for blurring. Each fuzzy domain uses seven fuzzy subsets to describe the input and output variable sizes: negative big (NB), negative medium (NM), negative small (NS), zero (Z), positive small (PS), positive medium (PM) and positive big (PB). Among them, NB adopts a Z-type membership function, PB adopts an S-type membership function, and the other subsets adopt a triangle membership function.

In order to adjust the PI parameters and perform fuzzy adjustment near the PI setting parameters, the domains of the fuzzy variables are set to: e = $[-0.6, -0.4, -0.2, 0, 0.2, 0.4, 0.6]$; de = $[-1.5e^7, -1e^7, -0.5e^7, 0, 0.5e^7, 1e^7, 1.5e^7]$; $\Delta K_p = [-6, -4, -2, 0, 2, 4, 6]$; and $\Delta K_i = [-300, -200, -100, 0, 100, 200, 300]$. Taking ΔK_p as an example, the membership function curve is shown in Fig. 6. The membership values of each subset are:

'NB': 'zmf', $[-6, -2]$;
'NM': 'trimf', $[-6, -4, 0]$;
'NS': 'trimf', $[-6, -2, 2]$;
'Z': 'trimf', $[-4, 0, 4]$;
'PS': 'trimf', $[-2, 2, 6]$;
'PM': 'trimf', $[0, 4, 6]$; and
'PB': 'smf', $[2, 6]$.

The ranges of the other variables are chosen by analogy.

The proportional coefficient K_p can increase the dynamic response of the system, and the integral coefficient K_i can be used to eliminate the steady-state error. Therefore, the parameters ΔK_p,ΔK_i are set as follows:

(1) When the current error $|e_{idq}|$ is large, in order to avoid overshoot and speed up the response, a larger ΔK_p and a smaller ΔK_i or ΔK_i =0 should be taken.

(2) When the current error $|e_{idq}|$ is small, in order to make the system have a good steady-state performance, take larger values of ΔK_p and ΔK_i.

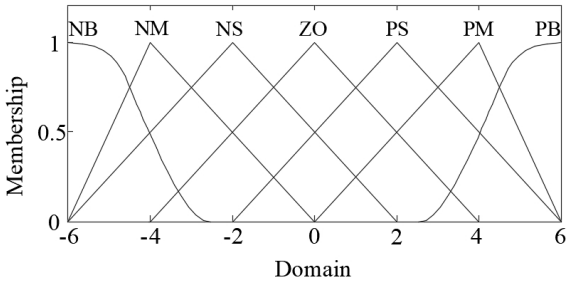

FIGURE 6. Membership function curve.

TABLE 1. Fuzzy PI control rule table.

$e;K_p,K_i;de$	NB	NM	NS	Z	PS	PM	PB
NB	*PB,NB*	*PB,NB*	*PM,NM*	*PM,NM*	*PS,NS*	*Z,Z*	*Z,Z*
NM	*PB,NB*	*PB,NB*	*PM,NM*	*PS,NS*	*PS,NS*	*Z,Z*	*NS,Z*
NS	*PM,NB*	*PM,NM*	*PM,NS*	*PS,NS*	*Z,Z*	*NS,PS*	*NS,PS*
Z	*PM,NM*	*PM,NM*	*PS,NS*	*Z,Z*	*NS,PS*	*NM,PM*	*NM,PM*
PS	*PS,NM*	*PS,NS*	*Z,Z*	*NS,PS*	*NS,PS*	*NM,PM*	*NM,PB*
PM	*PS,Z*	*Z,Z*	*NS,PS*	*NM,PS*	*NM,PM*	*NM,PB*	*NB,PB*
PB	*Z,Z*	*Z,Z*	*NM,PS*	*NM,PM*	*NM,PM*	*NB,PB*	*NB,PB*

(3) When the current error $|e_{idq}|$ and the error rate of change $|de_{idq}|$ are medium values and are the same number, it means that the controlled quantity develops away from the expected value, so a larger ΔK_p and an appropriate ΔK_i should be chosen. Otherwise, the values of ΔK_p and ΔK_i should be gradually reduced.

According to the above control law and expert experience, the general operator's practice shows the control rule table of ΔK_p and ΔK_i, as shown in Table 1.

The Mamdani type of Equation 29 is used as the fuzzy inference, and the weighted average of Equation 30 is used as the anti-fuzzification algorithm.

$$If\ e\ is\ A\ and\ de\ is\ B,\quad then\ \Delta K_p\ is\ C,\ \Delta K_i\ is\ D \tag{29}$$

$$u_0 = \frac{\sum_{i=0}^{n} u_i \mu_i(u_i)}{\sum_{i=0}^{n} \mu_i(u_i)} \tag{30}$$

where u_0 is the clear output, μ_i is the output variable value, and $\mu_i(u_i)$ is the corresponding membership.

IV. SIMULATION RESULTS ANALYSIS

In order to verify the validity and feasibility of the proposed algorithm, based on the above theory, an optimal power control system based on FFT for direct drive wave power generation without speed sensor technology is built by Matlab-Simulink simulation software. In this paper, based on EKF estimation of the generator position and speed, the approach provides feedback for the generator control. By using a vector control scheme, the expected electromagnetic force for maximum power is converted into the

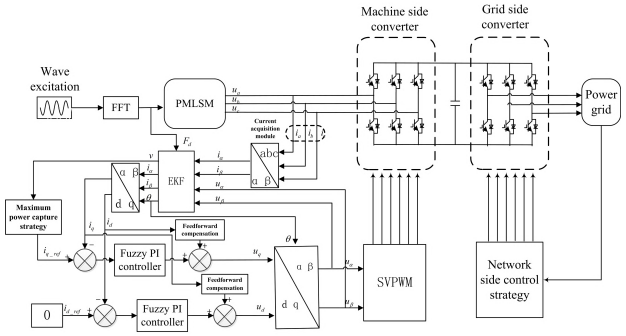

FIGURE 7. Model diagram of the direct drive wave power generation system.

TABLE 2. Selection of the generator parameters.

Parameters	Symbol	Value	Unit
d, q-axis inductance	L_dL_q	0.0082	H
Motor stator resistance	R_s	2.48	Ω
Total mass of the float	m_t	300	kg
Number of pole pairs	n_p	4	$pairs$
Permanent magnet flux	Φ_f	0.147	Wb
Damping coefficien	β_h	600	kg/s^2
Pole distance	τ	0.1	m

expected value of the stator current i_q. Through the parameter self-tuning fuzzy PI controller, voltage feed-forward compensation is used to decouple i_d and i_q, and the SVPWM method is used to generate the control pulse regulator side converter on/off state, which realizes the optimal power control of the generator and captures the maximum active power. Fig. 7 is a schematic diagram of the system mode, and the parameter selection is shown in Table 2. Considering that this paper only studies the control strategy of the machine-side converter, it has nothing to do with the grid-connected control, so the DC-side power supply is used instead of the side of the grid-side converter.

First, in order to verify the superiority of fuzzy PI control and the effectiveness of the EKF sensorless sensor technology, Equation 31 shows the wave excitation force that changes continuously over different time periods as the input. Based on the premise of keeping the simulation parameters of the model consistent, the PI controller and the parameter self-tuning fuzzy PI controller are used to control the wave generation system. The simulation results are shown in Figs. 8 and 9. It can be seen that both control results contain a large amount of ripple and chattering. The absolute value of the PI control tracking error is up to 0.49 A, while the fuzzy PI control tracking error is about 1/2 of that of PI control, which is about 0.25 A. At the 9th second, the excitation force and frequency suddenly change and decrease to 2/3 of the original values, the wave excitation force amplitude becomes 1/2 of

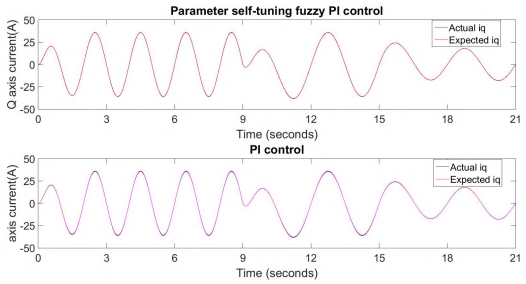

FIGURE 8. Two control methods for Q-axis current follow-up.

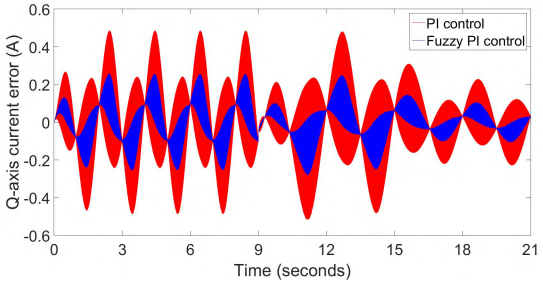

FIGURE 9. Comparison of the Q-axis current following error between the two control methods.

the original amplitude at the 15th second, and the system can be quickly adjusted to ensure synchronization of the control and accuracy. However, the control precision of the apparent fuzzy PI control is higher than that of simple PI control, and the control chattering is small.

$$F_w = \begin{cases} 2000sin(\pi t) & t \leqslant 9s \\ 2000sin(2\pi t/3) & 9s < t \leqslant 15s \\ 1000sin(2\pi t/3) & 15s < t \leqslant 21s \end{cases} \tag{31}$$

From the simulation results in Figs.10 and 11, it can be seen that the EKF velocity observer has a good speed and position prediction effect in the direct drive wave power generation system. During the first 9s, the speed is up to 1.8 m/s, the tracking error is less than 0.02 m/s, and the position estimation error is less than 0.1^0. During the period of $9 \sim 15s$, the direction and frequency change, but the speed and position size and the estimation error do not change greatly. During the period of $15 \sim 21s$, the speed error is less than 0.0045 m/s when the speed does not exceed 0.85 m/s. However, the speed sensorless technology used in [8] had a prediction error of up to 0.015 m/s at speeds up to 0.5 m/s. In contrast, the proposed observer has a smaller estimation error and a higher prediction accuracy.

Fig. 12 shows a 600 s irregular excitation force with clutter and an unknown frequency. The 128 s data is analyzed by a FFT to obtain the frequency distribution diagram as shown in Fig. 13. The main frequency components of the excitation force can be extracted from the figure: 0.25 Hz, 0.33 Hz, and 0.5 Hz. Compared with the actual component of Equation 32, although the frequencies corresponds to some differences in amplitude, the main components of the frequencies are basically consistent. In addition, the disturbance component

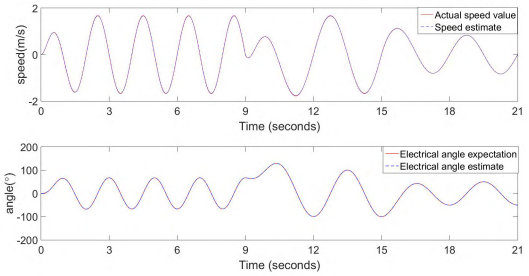

FIGURE 10. EKF observer speed and position estimation effect.

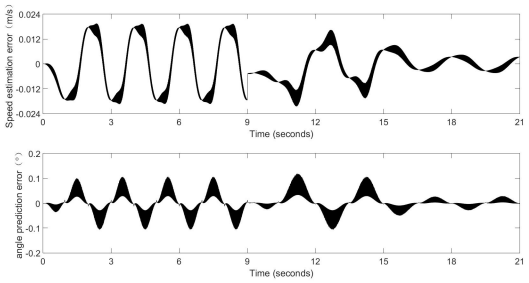

FIGURE 11. EKF observer speed and position estimation error.

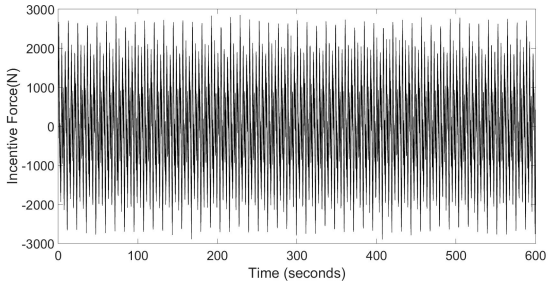

FIGURE 12. Actual irregular incentives.

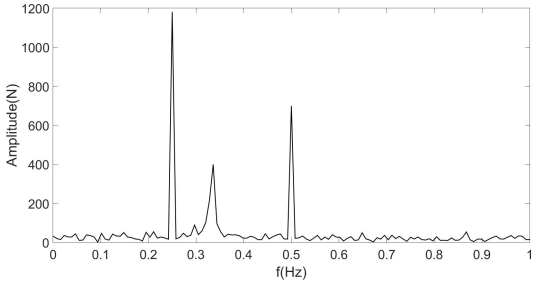

FIGURE 13. Spectrum distribution of the irregular wave excitation force.

can be filtered out, so the excitation force can be decomposed into a several regular sine wave. By using the maximum power capture control strategy of the regular wave, the optimal power control condition of the irregular wave excitation force is obtained by using the superposition principle.

$$F_w = 700sin(\pi t) + 500sin(2\pi t/3) + 1200sin(2\pi t/4) + 200randn(t) \quad (32)$$

In order to verify the advantages of the FFT algorithm in the energy conversion of irregular waves and considering the obviousness of the analysis and simulation speed, the 16 s

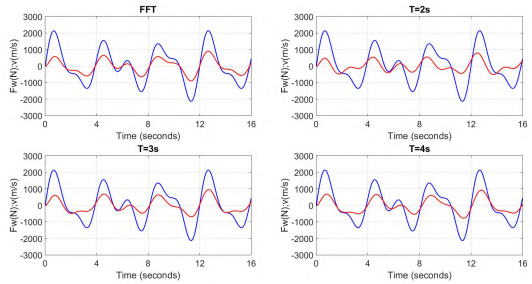

FIGURE 14. Wave excitation force and speed phase relationship.

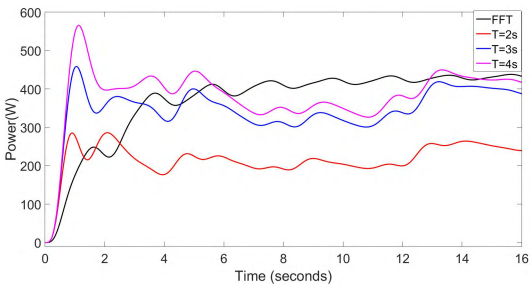

FIGURE 15. Wave energy capture average power comparison.

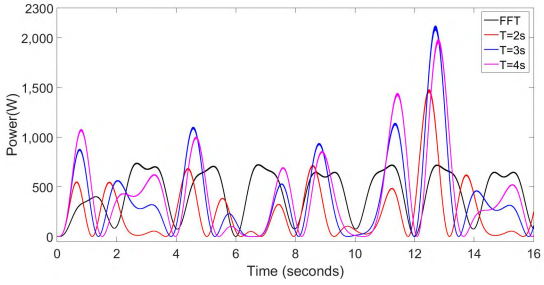

FIGURE 16. Wave energy capture instantaneous power comparison.

irregular wave is taken as the system input for the simulation analysis. The simulation result obtained by the FFT algorithm is compared with the result obtained by the single-frequency control condition, and at the same time, the speed is amplified by 500 times for an obvious comparison. The simulation results are shown in Figs. 14-16. It can be seen from Fig. 14 that the speed was obtained by the direct drive wave power generation system after the FFT analysis can always maintain the same phase as the irregular excitation force, satisfying the resonance phase requirement of the wave energy conversion device and the wave. However, the speed of the power generation system controlled by any single frequency cannot meet the conditions of being in phase with the excitation force, and it is difficult to maximize the wave energy conversion rate. The instantaneous and average values of the output active power of the power generation system in Figs. 15 and 16 also verify this conclusion.

V. CONCLUSION

In this paper, a direct drive wave power speed sensorless control system is built by combining a fuzzy self-tuning PI control algorithm and an EKF observer. The FFT algorithm

and the vector superposition principle are used to analyze the control conditions of the maximum power capture of an irregular wave excitation force, and then the power optimization of the system is realized. The simulation results show that the power consumption parameter of the generator and the EKF speed observer can realize speed estimation of the system. The estimation error meets the requirements, and the precision is high, which can effectively avoid the defect of the high maintenance cost of the speed sensor. Compared with the single-frequency algorithm, the FFT algorithm is obviously superior in the acquisition of the optimal power control condition for an irregular wave excitation force, can maintain in-phase conditions of the wave excitation force and the speed, and achieve a greater power output in the simulation result. At the same time, the fuzzy PI controller can dynamically adjust the PI parameters according to a change in the tracking signal and can track the given signal quickly and accurately under sudden changes in the motor speed direction, amplitude and frequency. Furthermore, the robustness and anti-interference ability are better, and method effectively avoids the insufficiency of the PI controller in achieving static tracking of a sinusoidal signal.

REFERENCES

[1] B. Alnajjab and R. S. Blum, "Estimating waveforms of ocean waves to enhance the efficiency of ocean energy conversion," *IEEE Trans. Sustain. Energy*, vol. 8, no. 1, pp. 179–191, Jan. 2017.
[2] Y. Zhou, G. Xu, S. Wei, X. Zhang, and Y. Huang, "Experiment study on the control method of motor-generator pair system," *IEEE Access*, vol. 6, pp. 925–936, 2017.
[3] S. R. K. Nielsen, Z. Zhang, M. M. Kramer, and J. Olsen, "Stability analysis of the Gyroscopic power Take-Off wave energy point absorber," *J. Sound Vib.*, vol. 355, pp. 418–433, Oct. 2015.
[4] O. Saeed, A. Wahyudie, T. B. Susilo, and H. Shareef, "Simple resonance circuit to improve electrical power conversion in a two-sided planar permanent magnet linear generator for wave energy converters," *IEEE Access*, vol. 5, pp. 18654–18664, 2017.
[5] J. Song, O. Abdelkhalik, R. Robinett, G. Bacelli, D. Wilson, and U. Korde, "Multi-resonant feedback control of heave wave energy converters," *Ocean Eng.*, vol. 127, pp. 269–278, Nov. 2016.
[6] A. Wahyudie and M. A. Jama, "Perspectives on damping strategy for heaving wave energy converters," *IEEE Access*, vol. 5, pp. 22224–22233, 2017.
[7] F. Wu *et al.*, "Modeling, control strategy, and power conditioning for direct-drive wave energy conversion to operate with power grid," *Proc. IEEE*, vol. 101, no. 4, pp. 925–941, Apr. 2013.
[8] M. I. Marei, M. Mokhtar, and A. A. El-Sattar, "MPPT strategy based on speed control for aWS-based wave energy conversion system," *Renew. Energy*, vol. 83, pp. 305–317, Nov. 2015.
[9] E. Abraham and E. C. Kerrigan, "Optimal active control and optimization of a wave energy converter," *IEEE Trans. Sustain. Energy*, vol. 4, no. 2, pp. 324–332, Apr. 2013.
[10] L. Hai, M. Göteman, and M. Leijon, "A methodology of modelling a wave power system via an equivalent RLC circuit," *IEEE Trans. Sustain. Energy*, vol. 7, no. 4, pp. 1362–1370, Oct. 2016.
[11] L. Yuan, F. Xiao, J.-Q. Shen, M.-L. Chen, Q.-M. Shi, and L. Quan-feng, "Sensorless control of high-power interior permanent-magnet synchronous motor drives at very low speed," *IET Electr. Power Appl.*, vol. 7, no. 3, pp. 199–206, Mar. 2013.
[12] O. Barambones and P. Alkorta, "Position control of the induction motor using an adaptive sliding-mode controller and observers," *IEEE Trans. Ind. Electron.*, vol. 61, no. 12, pp. 6556–6565, Dec. 2014.
[13] L.-Y. Lu, N. F. Avila, C.-C. Chu, and T.-W. Yeh, "Model reference adaptive back-electromotive-force estimators for sensorless control of grid-connected DFIGs," *IEEE Trans. Ind. Appl.*, vol. 54, no. 2, pp. 1701–1711, Mar./Apr. 2018.
[14] X. Liu, H. Yu, J. Yu, and L. Zhao, "Combined speed and current terminal sliding mode control with nonlinear disturbance observer for PMSM drive," *IEEE Access*, vol. 6, pp. 29594–29601, 2018.
[15] F. Alonge, T. Cangemi, F. D'Ippolito, A. Fagiolini, and A. Sferlazza, "Convergence analysis of extended Kalman filter for sensorless control of induction motor," *IEEE Trans. Ind. Electron.*, vol. 62, no. 4, pp. 2341–2352, Apr. 2015.
[16] J.-L. Shi, T.-H. Liu, and Y.-C. Chang, "Position control of an interior permanent-magnet synchronous motor without using a shaft position sensor," *IEEE Trans. Ind. Electron.*, vol. 54, no. 4, pp. 1989–2000, Jun. 2007.
[17] L. Sheng, W. Li, Y. Wang, M. Fan, and X. Yang, "Sensorless control of a shearer short-range cutting interior permanent magnet synchronous motor based on a new sliding mode observer," *IEEE Access*, vol. 5, pp. 18439–18450, 2017.
[18] C. Yang, T. Ma, Z. Che, and L. Zhou, "An adaptive-gain sliding mode observer for sensorless control of permanent magnet linear synchronous motors," *IEEE Access*, vol. 6, pp. 3469–3478, 2018.
[19] B. Chappuis, S. Gavin, L. Rigazzi, and M. Carpita, "Speed control of a multiphase active way linear motor based on back EMF estimation," *IEEE Trans. Ind. Electron.*, vol. 62, no. 12, pp. 7299–7308, Dec. 2015.
[20] D. Su, C. Zhang, and Y. Dong, "Finite-state model predictive current control for surface-mounted permanent magnet synchronous motors based on current locus," *IEEE Access*, vol. 5, pp. 27366–27375, 2017.
[21] S. Du, J. Hu, Y. Zhu, and M. Zhang, "A hall sensor-based position measurement with on-line model parameters computation for permanent magnet synchronous linear motor," *IEEE Sensors J.*, vol. 18, no. 13, pp. 5245–5255, Jul. 2018.
[22] J. Hu, J. Zou, F. Xu, Y. Li, and Y. Fu, "An improved PMSM rotor position sensor based on linear Hall sensors," *IEEE Trans. Magn.*, vol. 48, no. 11, pp. 3591–3594, Nov. 2012.
[23] J. Kim, S. Choi, K. Cho, and K. Nam, "Position estimation using linear Hall sensors for permanent magnet linear motor systems," *IEEE Trans. Ind. Electron.*, vol. 63, no. 12, pp. 7644–7652, Dec. 2016.
[24] I. M. Alsofyani and N. R. N. Idris, "Simple flux regulation for improving state estimation at very low and zero speed of a speed sensorless direct torque control of an induction motor," *IEEE Trans. Power Electron.*, vol. 31, no. 4, pp. 3027–3035, Apr. 2016.
[25] Y. C. Shi, K. Sun, L. P. Huang, and Y. D. Li, "Online identification of permanent magnet flux based on extended Kalman filter for IPMSM drive with position sensorless control," *IEEE Trans. Ind. Electron.*, vol. 59, no. 11, pp. 4169–4178, Nov. 2012.
[26] F. Wu, X. P. Zhang, P. Ju, and M. J. H. Sterling, "Optimal control for AWS-based wave energy conversion system," *IEEE Trans. Power Syst.*, vol. 24, no. 4, pp. 1747–1755, Nov. 2009.
[27] J. Yu, P. Shi, W. Dong, B. Chen, and C. Lin, "Neural network-based adaptive dynamic surface control for permanent magnet synchronous motors," *IEEE Trans. Neural Netw. Learn. Syst.*, vol. 26, no. 3, pp. 640–645, Mar. 2014.
[28] L. Sheng, G. Xiaojie, and Z. Lanyong, "Robust adaptive backstepping sliding mode control for six-phase permanent magnet synchronous motor using recurrent wavelet fuzzy neural network," *IEEE Access*, vol. 5, pp. 14502–14515, 2017.
[29] Z. Meng, H. Liang, Y. Bai, Q. Guoqiang, M. Rui, and H. Fang, "Speed sliding-mode control for wave power generation system of float-type," *Proc. CSU-EPSA*, vol. 28, no. 11, pp. 130–134, 2016.

JUNHUA YANG was born in Henan, China, in 1965. He received the B.S. degree from the South China Institute of Technology, in 1985, and two Ph.D. degrees from the South China University of Technology, in 1991 and 2006, respectively. He is currently a Professor with the School of Automation, Guangdong University of Technology, Guangzhou.

His research interests include electrical appliances and their control and new energy generation control.

BAOZHOU HUANG was born in Jieyang, China, in 1995. He received the B.S. degree in electrical engineering and automation from the Guangdong University of Technology, Guangzhou, China, in 2017, where he is currently pursuing the M.S. degree in electrical engineering.

His current research interest includes optimal control of speed sensorless technology for direct drive wave power systems.

HUI SHEN was born in Henan, China, in 1969. He received the B.S. and M.Eng. degrees from North China Electric Power University, Beijing, China, in 1991 and 2011, respectively. He is currently a Senior Engineer of the Maintenance Company of Henan Electric Power Corporation, Zhengzhou, China. His research interests include power system operation and control.

DONGSHEN XIE was born in Guangzhou, China, in 1993. He received the B.S. degree in electrical engineering and automation from the Changchun University of Science and Technology, Changchun, China, in 2016. He is currently pursuing the M.S. degree in electrical engineering from the Guangdong University of Technology, Guangzhou.

His current research interests include chaotic phenomenon analysis, and control of linear motors and control of new energy generation.

FENGJUN XIONG was born in Meizhou, China, in 1993. He received the B.S. degree in electrical engineering and automation from the Guangdong University of Technology, Guangzhou, China, in 2016, where he is currently pursuing the M.S. degree in electrical engineering.

His current research interests include chaotic system control and MPPT of wave energy converters.

SILING LU was born in Jieyang, China, in 1994. She received the B.S. degree in electrical engineering and automation from the Guangdong University of Technology, Guangzhou, China, in 2017, where she is currently pursuing the M.S. degree in electrical engineering from the Guangdong University of Technology, Guangzhou, China.

Her current research interest includes research on direct drive wave power system control.

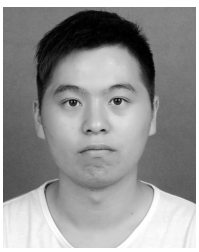

HAIFENG CHEN was born in Huizhou, China, in 1993. He received the B.S. degree in electrical engineering and automation from Foshan University, Foshan, China, in 2017. He is currently pursuing the M.S. degree in electrical engineering from the Guangdong University of Technology, Guangzhou, China.

His current research interest includes research on direct drive wave power system maximum power tracking.